The Effect of Composition and Thickness on the Mechanism and Kinetics of Filiform Corrosion occurring on Zinc-Aluminium-Magnesium coated steel

N. Wint [a,*], D. Eaves [a], G. Williams [a], H. N. McMurray [a].

[a] *Materials Research Centre, College of Engineering, Swansea University, Bay Campus, Fabian Way, Crymlyn Burrow, Swansea, UK, SA1 8EN*

Abstract:

The effect of coating thickness and composition on the kinetics of acetic acid-induced filiform corrosion (FFC) on Zinc-Aluminium-Magnesium (ZAM) coated steel is investigated. Scribe defects are created in organic coatings applied to ~10 µm coatings of varying composition (1-6 wt.%. Al, 1-3 wt. % Mg), and fixed composition (Zn-1.5 wt. % Al- 1.5 wt.% Mg) but varying thickness (5-27 µm). FCC decreases with increasing Al (at fixed wt. % Mg) and thickness. A linear trend exists between thickness and iron exposure time. Findings are consistent with FFC advancing via a penetrative coating mechanism whereby exposed iron couples to the coating.

Keywords; A Steel A Magnesium A Metal Coatings C Atmospheric Corrosion C Polymer Coatings.

*Corresponding author:
E-mail address: n.wint@swansea.ac.uk

1. Introduction

Metallic coatings based on Zn alloyed with Al and Mg (e.g. SuperDyma® Zn-11 wt.%Al-3 wt.% Mg) have been used for the cathodic protection of steel for several decades. In more recent years, the reduced corrosion-driven mass loss associated with zinc-aluminium-magnesium (ZAM) coated steel (compared to Zn coated steel of similar thickness) [1] has helped drive an increase in the production of Zn coatings which incorporate lower amounts of alloying addition (~ 0.1-3.5 wt. % Mg and 0.1-3.5 wt. % Al) and can therefore be used for more widespread applications. However, a large proportion of the ZAM hot dip galvanised steel used in service is overcoated with organic coatings. Organic coating failure can occur in the presence of penetrative coating defects which allow aggressive electrolytes to come into contact with the metal substrate [2]. Cathodic disbondment and filiform corrosion (FFC) are two specific modes of corrosion driven organic coating delamination arising from differential aeration phenomena, which both occur under atmospheric corrosion conditions at high relative humidity [2]. In the case of cathodic delamination, it is cathodic oxygen reduction reaction (ORR) which is responsible for disbondment of the organic coating from the metal substrate, and only group I cations possess the hydrolytic stability and solubility necessary to support the strongly alkaline electrolyte necessary [2-4]. Whilst organic coating failure via cathodic delamination has been reported to occur on zinc [5-9], $MgZn_2$ (one of the predominant phases present within ZAM alloys) [10-13] has been shown to resist cathodic delamination [14-17]. This finding was (primarily) attributed to an inversion of the normal difference in electrochemical potential observed between the anodically active defect and the intact organic coated $MgZn_2$ surface [14-17]. Elsewhere, 1.5 wt. % Al, 1.5 wt. % Mg coatings were found to exhibit a high resistance to corrosion driven delamination of an organic (PVB) overcoat film [18]. This finding was believed to be a result from the presence of Mg-Zn and Mg-Al-Zn eutectic phases in the coating microstructure. These phases are predicted to have low activity for cathodic O_2 reduction. The presence of eutectic therefore renders the principle O_2 reduction cathode (primary zinc) discontinuous and inhibits the movement of the cathodic disbondment front [18].

In comparison, acetic acid, CH_3COOH (which will from this point be referred to as HAc) induced FFC has recently been shown to be an important mode of the corrosion driven organic coating failure on ZAM [18]. FFC is a form of anodic disbondment which occurs when an aggressive electrolyte comes into contact with the metal substrate at defects in the organic coating [2]. FFC presents as tracks of corrosion product which propagate under the organic coating and lengthen with time. The electrolyte is contained within the filament head at which anodic dissolution occurs [19-21]. The anodic dissolution is coupled to the cathodic ORR, which occurs primarily at the rear of the head where water-insoluble metal oxides and hydroxides are formed. Williams and McMurray observed an area of cathodic delamination preceding filiform corrosion but contest its role as a primary cathode and claim it plays no role in the mechanism of filiform advance [22]. Watson used in-situ timelapse optical microscopy to gain a mechanistic understanding of filiform in a dual compartment cell in which independent control of the areas surrounding the head and the tail. Watson confirms presence of a cathode around the head, suggesting that the annulus of dark corrosion product observed is the result of cathodic activity, but states that the constant filament speed observed suggests there is no mass transport limitation on propagation [23]. FFC then propagates via differential aeration [19-24]. Although $FeCl_2$, NaCl and HCl have been shown to act as initiators of FFC on iron [22-23, 25] and aluminium [24, 26-32], and magnesium [33], only HAc has been found to reliably and reproducibility produce FFC on ZAM coatings [18]. HAc is known to be one of the most ubiquitous initiators of atmospheric corrosion which occurs on materials exposed to indoor environments and it is emitted during several important technological and biological processes [34-42]. Although FFC has not, as far as is known, been observed to occur on ZAM exposed to HAc when used within indoor environments, the mechanism of failure via FFC is of scientific and industrial interest. In this paper we present an investigation into the effect of both ZAM coating thickness, and composition, on HAc induced FFC, with the aim of further elucidating the mechanism by which it occurs.

The principal component making ZAM susceptible to HAc induced FFC is assumed to be $MgZn_2$ (present in the eutectic phases of the microstructure), an intermetallic which has been shown to be attacked at the front of an advancing filament head [18]. FFC advancement is then hypothesized to proceed by a penetrative through coating mechanism in which anodic dissolution of the Mg rich phases allows O_2 percolation to Fe substrate, which acts as the FFC cathode. If this hypothesis were true, then an inverse relationship would exist between coating thickness and FFC area rate (i.e. the increased charge required for dissolution of thicker coatings will result in reduced rates of propagation). The effect of a systematic change in coating thickness (coating weight), on FFC growth kinetics, can therefore be studied with the aim of confirming the mechanism by which FFC propagates on ZAM.

A question then arises as to whether the ZAM composition may be changed in such a way as to decrease the rate of iron exposure. For example, Al resists the action of HAc at room temperature and has been used for the transportation and storage of acetic acid. It therefore seems plausible that HAc induced dissolution of ZAM may be decreased by increasing the Al content [43]. In comparison, magnesium acetate is highly soluble in water [44] and zinc hydroxyacetate salts [44-45] tend to decompose through hydrolysis at room temperature, releasing acetate. Alloying of Zn based coatings, with elements such as Al and Mg, results in the creation of different phases of different sizes, shapes, distribution and proportion, and small differences in composition result in variations in the behavior of localized corrosion [46-47]. Localized attack results in non-uniform distribution of pH and electrolyte composition, which in turn determine the stability of the corrosion product formed [48-49].

The effect of coating composition on the kinetics and mechanism of corrosion on bare galvanized steel (without an organic overcoat) has been thoroughly studied in a range of environments [1, 10-11, 14-17, 46-70]. Phases which contain Al are considered stable compared to the zinc matrix [11, 50-51, 56] whilst Mg containing phases (e.g. $MgZn_2$ and Mg_2Zn_{11}) preferentially corrode [1, 11, 50-51, 56]. $Mg(OH)_2$, formed by reaction of the Mg^{2+} ions (released during dissolution) and OH^- ions (produced at the cathode), replaces zinc (hydr)oxide on the ZAM surface [14, 52, 65]. The presence of $Mg(OH)_2$ is believed to reduce the ORR rate [14, 55], and to 'buffer' the electrolyte pH such as to stabilize protective hydrozincite ($Zn_5(CO_3)_2(OH)_6$) and simonkolleite ($Zn_5(OH)_8Cl_2 \bullet (H_2O)$) [50, 54]. The addition of Al to Zn alloy coatings results in a modification to the morphology and stability of zinc corrosion product (ZnO) [49], which becomes more compact and enriched in aluminium [62] and the corrosion product formed on Zn-Al-(Mg) coatings has been shown to be dependent on Al^{3+} concentration [70]. Aluminates, can also react with Mg^{2+}ions to form layered double hydroxides (LDH) which remain stable up to pH 12 [1, 50, 52, 62]. The mass lost from HDG and various Zn-Al, Zn-Mg and Zn-Al-Mg coatings, pre-deposited with NaCl and stored in humid air, has been shown to be lowest for the most highly alloyed samples [55].

In comparison, work pertaining to the ability of Zn alloys to resist corrosion driven organic coating failure is limited, and primarily focuses on Zn-Mg alloys. For example, the cathodic delamination of PVB from PVB Zn-Mg films of varying composition has been investigated using in situ Kelvin probe [60]. Whilst cathodic disbondment was observed at Mg compositions of ≤5 wt. % w/w, Zn–Mg coatings in the range 10–25 wt. % were shown to resist delamination for periods of up to 48 h. In comparison, Mg compositions of ≥ 12 wt. % were instead susceptible to coating failure by anodic undermining [60]. A thorough investigation into the effect of ZAM composition on the corrosion of organically coated ZAM has not been completed. It has also been shown that changing the amount of Al and Mg within the range 1–2 wt. % does not result in any major differences in scribe creep [71]. The current work therefore aims to address the lack of knowledge in how ZAM composition influences the rate of organic coating failure rates, especially when anodic disbondment is the prevailing one.

The aim of this paper is two-fold. Firstly, to confirm that the rate of FFC propagation on ZAM is proportional to the time to iron (substrate) exposure. Secondly, to determine whether the relative amount of each ZAM element can be modified in such a way as to decrease the rate of iron exposure, and thus FFC propagation. In so doing Zn-1.5 wt.% Al-1.5 wt. % Mg coating weight (thickness) is systematically varied and FFC is initiated via the application of small, controlled, quantities of 1.5 mol.dm^{-3} HAc to a penetrative defect in the polyvinyl butyral co-vinyl alcohol-co-vinyl acetate (PVB) coating, followed by incubation at a controlled relative humidity. The rate of FFC propagation is determined as a function of ZAM coating weight (thickness) and correlated with iron substrate exposure time, as determined by immersing the different coated samples in HAc for varying periods of time. A similar study is completed whereby the Al content of a 10 µm thick ZAM coating is changed between 1-6 wt.%. Al. The composition range used is representative of the compositions which are commercially available, and as such, the amount of Mg contained within the alloy also varies in some cases. Nevertheless, it is still possible to complete a systematic investigation into the effect of wt. % Al, on FFC rate.

2. Materials and Methods

2.1 Materials

Two sets of Zn-Al-Mg coated steel were supplied by Tata Steel. In the case of the first set, the 0.7 mm gauge mild steel was coated with a ~10 μm thick (140 $g.m^{-2}$) ZAM layer of varying composition (see Table 1 which also gives denominations which will be used for the remainder of this work) on each side. For the second set the coating composition (1.5Al-1.5 Mg) was kept the same whilst the coating weight (thickness) was varied between 70 $g.m^{-2}$ and 350 $g.m^{-2}$ (Table 2). Experimental coupons were cut from a larger sheet and were 5 cm × 5 cm in size. They were cleaned using an aqueous slurry of 5 μm polishing alumina, rinsed with distilled water, degreased in hexane and allowed to air dry. All solvents and reagents used were provided by the Sigma-Aldrich Chemical Company and of analytical grade.

(Table 1)

(Table 2)

2.2 Methods

Materials Characterisation; A Hitachi TM3000 SEM with integrated Quantax 70 EDX Analyser was used to obtain both SEM images of the various uncorroded ZAM microstructure and images of the surface post-corrosion in HAc. PVB was mechanically peeled from the samples following removal from the humidity chamber. Any loose corrosion product present was removed from the corroded samples during ultrasonication in a non-polar hydrocarbon (hexane) for 10 minutes prior to SEM.

Filiform Corrosion; Insulating tape was applied to coupons in two parallel stripes. The tape acted as a height guide onto which PVB was bar-cast before being allowed to dry in air (30 µm dry film thickness) [22, 23, 28-29, 33]. A scalpel blade was used to create 10 mm long linear scribe penetrative coating defects to which aliquots (2 µL) of 1.5 mol.dm^{-3} HAc (pH~2) were applied using a micro-syringe. Coupons were then placed in an experimental chamber within which the relative humidity (RH) was maintained at 93 % using reservoirs of saturated $Na_2SO_4 10H_2O$ [22, 23, 28-29, 33]. The temperature was held constant at 25 °C. A Canon EOS was used to take digital optical images of the sample surface once per week, at which point the chamber air was refreshed. Sigma Scan Pro 5 image analysis software was used to take measurements from the images and obtain values of FFC corroded area. Calibration of the image analysis software was completed by specifying a pre-measured distance between two points in the image and inputting the real distance. Measurements of corroded area were taken from four individual scribes (2 samples each with 2 scribes) for each coating composition and coating weight.

3. Results and Discussion

3.1 Materials Characterisation

Figure 1 shows cross sections of the four 1.5Al- 1.5 Mg coatings of varying coating weight. The mean thickness of each coating was determined by taking several measurements across the coating from five different images and are shown in Table 2. Zinc dendrites, binary and ternary eutectic phases are present in all coatings at approximately equal proportions.

Figure 2 shows SEM backscatter images of the surface of the four ZAM alloys before immersion in HAc (0 hours). Each of the samples were supplied with similar ZAM coating weights, giving a roughly constant thickness for each different composition. The area percentage, along with the composition, of each phase present are shown in Table 3. Values shown are based on measurements taken on five different areas. Both 1Al-1Mg (Figure 2a) and 1.5Al-1.5Mg (Figure 2b) alloys coating consists of zinc dendrites (Zn HCP) within a coarse binary eutectic phase and a finer ternary eutectic. The binary eutectic consists of zinc and $MgZn_2$ lamellae and the ternary eutectic consists of zinc, a zinc rich aluminium fcc phase and $MgZn_2$ [10, 72]. By comparing Figure 2a and Figure 2b it can be seen that increasing the alloying additions of magnesium and aluminium increases the proportion of binary and ternary eutectic from ~ 10 % to ~ 30 % and from ~10 % to ~ 40% respectively. In comparison, the proportion of primary zinc dendrites decreases from ~ 80 % to ~ 30 % and they become smaller in size (~ 50 μm to < 10 μm). Figure 2c shows the surface of the 3Al-3Mg alloy. A fourth dendritic, zinc rich aluminium phase, (~ 10 %) forms from the aluminium which has been excluded from the primary zinc dendrites during solidification. The composition of this phase, as determined using EDX, (Table 3) is Al (21wt. %) and Zn (79 wt.%) with very little magnesium. The phase identified is consistent with an fcc Zn-rich (~60-80 %) Al phase observed in Zn-Al-Mg coatings using wavelength dispersive x-ray spectrometry [73]. Figure 2d shows the surface of the 6Al- 3Mg alloy. Virtually no primary zinc is formed in the coating, which consists primarily of ternary eutectic (~70 %) and binary eutectic (~ 10 %). This excess of aluminium, above that required for formation of the ternary eutectic, means there is a significant increase in the amount of the fourth Zn-Al phase to ~ 20 %.

(Figure 1)

(Figure 2)

(Table 3)

3.2 Post Corrosion Surface Characterisation

The effect of differential aeration in FFC occurring on 1.5Al-1.5Mg has been found to be reinforced by the preferential anodic dissolution of the magnesium-rich eutectic phases which produces pathways in the ZAM coating to the iron substrate [18]. The exposed iron is then able to galvanically couple to ZAM coating, increasing the driving force for filament advance. It therefore seems reasonable to propose that a change in the exact composition of the ZAM coating will affect the time to iron exposure and that FFC will be significantly reduced in the case that exposure of the substrate is prolonged.

The effect of coating composition on both the ability of HAc to attack the ZAM coating microstructure, and the time to iron exposure, was further investigated by immersing ZAM coated coupons in 0.1 mol.dm^{-3} HAc. Samples were removed from the electrolyte hourly, rinsed with distilled water and immersed in hexane for 5 minutes in an ultrasound bath to mechanically remove corrosion products. Figure 2a shows backscatter SEM images, and the corresponding EDS maps, of the 1Al-1Mg surface obtained after various times of immersion. The change in wt. % of each element with time, as measured using EDS, is shown clearly for each coating type in Figure 3. The time dependent Mg wt. % (Figure 3a) follows a similar trend for each alloy; a sharp decrease followed by a plateau. The time taken for the value to plateau increases from 1 hour in the case of 1Al-1Mg, to approximately 5 in the case of 6Al- 3Mg. An increase in Al (which does not dissolve in HAc) occurs over the experimental time period as the surface becomes enriched. The time taken for the value to plateau approximately doubles from 2 hours to ~ 4 hours for the 1Al-

1Mg and 6Al- 3Mg respectively**.** The Fe wt.% (Figure 3c) increases sharply after a time period, the length of which depends upon the initial amount of Al and Mg present within the coating. For 1Al-1Mg coatings, the Fe content reaches 81.2 wt. % after 3 hours of immersion. In comparison the Fe content of the 1.5Al-1.5Mg coating is 4.1 wt. % after 3 hours and does not reach 82.2 wt. % until after 4 hours of immersion. The corresponding SEM and EDS images in Figure 2b show that iron is exposed more quickly in the eutectic regions compared to regions in which zinc dendrites are present. The EDS maps for the 3Al- 3Mg (Figure 2c) and 6Al-3Mg (Figure 2d) coatings show that iron is exposed more quickly in eutectic regions compared to those in which the Zn rich Al phase is present.

(Figure 3)

Figure 4 shows SEM images of the cross section of both a 1Al-1Mg and 6Al-3Mg coating after 15 seconds immersed in 0.8 mol.dm^{-3} HAc. This experiment was conducted to compare the dissolution rate of two coatings and a higher concentration of HAc was used than during previous studies in order to reduce the experimental time. The images clearly show the 1Al-1Mg coating almost entirely dissolves after 15 seconds and much of the iron substrate is left exposed. In comparison, the undissolved coating forms a tortuous path to the substrate in the case of the 6Al-3Mg coating.

(Figure 4)

The EDS technique used here is associated with an interaction volume and it is therefore not clear whether the increase in Fe observed in Figure 3 results from the active exposure of substrate Fe or that buried under residual Zn or corrosion product. However, what is clear is that the degree to which the Fe substrate is covered decreases during immersion in HAc, and from Figure 4 it is further evident that percolating pathways to the substrate would become open prior to complete removal of the ZAM coating. The presence of such pathways allows the Fe surface to contribute to cathodic activity, this in turn increasing the FFC propagation rate. Follow the immersion of coatings with increased Al content (Figure 4b) the extent of pathway formation is reduced, and it follows that the influence of the Fe substrate in contributing to cathodic activity also decreases.

A similar study was completed to determine the effect of 1.5Al-1.5Mg coating weight (thickness), on time to iron exposure. The ZAM coating weight (thickness) was systematically changed from 70 $g.m^{-2}$ to 350 $g.m^{-2}$ and samples were immersed in 0.1 $mol.dm^{-3}$ HAc. Figure 5 shows that the time to iron (substrate) exposure changes almost linearly as a function of coating weight (thickness).

(Figure 5)

3.3 Filiform Corrosion Study

Effect of coating composition; A systematic study was conducted with the aim of determining the effect of ZAM coating composition on the kinetics of FFC. In so doing 2μL aliquots of 1.5 $mol.dm^{-3}$ HAc (which has previously been shown to initiate FFC quickly and reproducibly) [18] were injected into the scribed PVB coating defect. Figure 6a shows representative optical images of PVB coated 1.5Al-1.5Mg samples taken 1, 4 and 8 weeks after injection of 1.5 $mol.dm^{-3}$ HAc into a coating scribe. The FFC filaments appear white against the dark substrate. FFC is observed in the first week following initiation (Figure 6a) and filaments extend perpendicular to the direction of the scribe. As time progresses these filaments propagate away from the defect and the FFC corroded area increases considerably after 4 and 8 weeks. Similar images were acquired for each of the ZAM coating compositions; 1.5Al-1.5Mg (Figure 6b), 3Al-3Mg (Figure 6c) and 6Al-3Mg

(Figure 6d). There is a delay in FFC initiation on 1.5Al-1.5Mg and FFC is not observed one week after initiation (Figure 6b). After 4 weeks FFC is observed and the FFC corroded area has increased after 8 weeks. The delay in FFC initiation is prolonged on 3Al-3Mg and FFC is not observed after 4 weeks (Figure 6c). Finally, in the case of 6Al-3Mg coatings FFC is not observed over the entire 8-week period and the experimental time period was extended to 20 weeks, after which FFC was still not observed.

(Figure 6)

The time dependent total corroded area on each type of sample was obtained by digital image analysis of the whole filament population. Figure 7 and Table 4 show total corroded area as a function of time for various ZAM coating compositions. For the sake of legibility, the confidence intervals (which correspond to ± one standard deviation on the mean of four measurements) given in Table 4 are not reproduced in Figure 7. Linear extrapolation gives a non-zero x-axis intercept corresponding to a composition dependent initiation period (delay). This initiation time increases from ~2 weeks for 1.5Al-1.5Mg to ~3 weeks for 3Al-3Mg. Following initiation, total corroded area increases linearly with time and the mean corroded area rate for each ZAM composition was obtained using linear regression (solid lines) and are shown in Table 4. A rate of 0.28±0.01 mm.week^{-1} was obtained for 1Al-1Mg , 0.27±0.01 mm.week^{-1} for 1.5Al-1.5Mg , 0.10±0.01 mm.week^{1} for 3Al-3Mg and 0.05±0.01 mm.week^{-1} for 6Al-3Mg . The linearity of the area-time plots shown indicate that FFC propagates at an approximately constant rate, this finding being consistent with FFC in general and the notion that acetate (and therefore electrolyte volume) is conserved in the propagating FFC head [2, 19-20]. The fact that the kinetics are linear also implies that the main cathodic site remains at a constant distance away from the leading anodic head [28]. If this were not the case, and the cathodic site was constrained to the defect, then the rate of filament progression would be controlled by the migration of ions in the underfilm electrolyte, and parabolic kinetics would become established. Linear kinetics are observed in all cases, indicating that the rate limiting process does not change with composition,

(Figure 7)

(Table 4)

Figure 8 and Table 5 show total corroded area as a function of time for 1.5Al-1.5Mg coatings of varying coating weight (thickness). For coating weights of both 70 g.m^{-2} and 100 g.m^{-2} FFC initiates within 1 week and proceeds to propagate at an approximately linear rate. For coating weights of 140 g.m^{-2} FFC does not initiate for 2 weeks, this increasing to 3 weeks in the case of the highest coating weight (350 g.m^{-2}). The mean corroded area rate for each coating weight was obtained using linear regression (solid lines) and are shown in Table 5. A rate of 0.31±0.01 mm.week^{-1} was obtained for 70 g.m^{-2}. Similar rates were obtained for coatings of coating weight between 100 and 200 g.m^{-2}. For coating weights 275 g.m^{-2} and 350 g.m^{-2} the rates obtained were 0.16±0.01 mm.week^{-1} and 0.11±0.01 mm.week^{1} respectively.

(Figure 8)

(Table 5)

In both Figure 7 and Figure 8 the initiation time (delay) is believed to correspond to a process whereby the HAc initiant becomes converted to a metal acetate salt solution which becomes the filament head electrolyte. Whilst it is likely that 1.) the FFC filament head

HAc concentration is significantly lower than the 0.1 mol.dm^{-3} HAc used during immersion experiments (Figure 2) and that 2.) the acetate anions present will be associated with salts of magnesium, zinc and aluminum, it is assumed that HAc induced FFC propagates via a process of magnesium-rich ($MgZn_2$ in the eutectics) phase dissolution and iron exposure [18]. The anodic attack of $MgZn_2$ (at least initially) at the front of the filiform head could then galvanically couple with cathodic ORR occurring either on zinc, or the iron substrate (which will be exposed during dissolution of the coating), at the rear filament head. The high solubility of magnesium acetate would ensure that it is retained within the advancing electrolyte head. However the Mg^{2+} ions, which are released during the dissolution of Mg rich phases migrate toward the tail, can react with the OH^- ions produced at the cathode to form $Mg(OH)_2$ once the solubility product *Ksp* (1.8 x 10-11 mol^3.dm^{-9}) [74] is exceeded. If FFC advancement were to proceed via this penetrative through coating mechanism, then the linear relationship observed between coating thickness and time to iron exposure (Figure 5) would be reflected by an inverse relationship between coating thickness and FFC area rate (i.e. the increased charge required for dissolution of thicker coatings will result in reduced rates of propagation). Indeed, Figure 9 shows an approximately linear inverse relationship between the reciprocal of coating thickness and FFC corroded area rate.

(Figure 9)

With this in mind, it may be assumed that the relationship between iron exposure time and coating composition (Figure 3 and Table 4) manifests in a correlation between coating composition and the FFC performance of coatings. That is to say, the superior resistance to FFC, demonstrated by coatings with higher levels of Al (notably in the case that the Mg content is fixed at 3 wt. %), correlates well with time to iron exposure. These findings are consistent with the increased corrosion performance exhibited by Galfan coatings (5 wt.% Al), compared to Zn HDG, when both were subject to NaCl and cyclic wet/dry conditions within a laboratory, as well as after 5 years of exposure to marine environment [75]. Approximately half the amount of zinc was released from a pure zinc sheet compared to Galfan [75]. The zinc and aluminium hyd(oxides) initially formed were shown to react to form Hydrozincite ($Zn_5(CO_3)_2(OH)_6$) and Hydrotalcite ($Zn_6Al_2(OH)_{16}CO_3{\cdot}4H_2O$) [75]. High chloride deposition rates resulted in the subsequent formation of hydroxychlorides, Simonkolleite ($Zn_5(OH)_8Cl_2{\cdot}H_2O$) on bare Zn metal, and $Zn_2Al(OH)_6Cl{\cdot}2H_2O$ and/or $Zn_5(OH)_8Cl_2{\cdot}H_2O$ on the Zn–Al coatings [75]. The improved corrosion performance of Galfan was attributed to the improved barrier properties of corrosion products formed in chloride-rich environments, and $Zn_6Al_2(OH)_{16}CO_3{\cdot}4H_2O$ was believed to govern the long-term runoff rate of zinc from Galfan [75].

However, it should, at this point, be considered that the difference in Al content of the coatings used during this work is often accompanied by a change in Zn and Mg wt.%. Therefore, although it is well possible that the effect of composition on FFC corroded area is linked to the Al content, the only pair of samples with identical Mg content (and still significantly different microstructure) are 3Al-3Mg and 6Al-3Mg. In all other cases, both Al and Mg concentrations, as well as the microstructure, change.

In summary, this work establishes that small variations in composition can have significant effects on the susceptibility of ZAM to anodic mechanisms of organic coating failure. The composition of such coatings should therefore be optimized to ensure that the benefits afforded by the addition of Mg [14, 50, 52, 54-55, 65], and Al, allow for maximum corrosion resistance in a range of different scenarios, including, as demonstrated here, when the surface is coated with a protective organic layer. When considering inhibition of FFC by Al additions in the coating layer, an "indirect" contribution arising from Al and Mg ions inhibiting the ORR on exposed iron cannot be ruled out. A similar effect has been observed at the cut edge of galvanized steel due to a direct modification of the iron oxide by zinc cations, which is enhanced by magnesium cations and causes an inhibition of oxygen reduction directly on the steel [76]. Nevertheless, the simplest explanation of the effect is that it results "directly" from the insolubility of Al in aqueous HAc and the microscopically observed resistance of Al-rich phases to the experimental FFC electrolyte. With this in mind, it should also be remembered that such coatings can corrode via a variety of mechanisms, most notably cut edge corrosion, and this (alongside factors such as environmental conditions) should be considered during coating design.

5. Conclusions

This paper describes a systematic study into the effect of Zn-Al-Mg (ZAM) coating thickness and composition on the mechanism and kinetics of filiform corrosion (FFC).

- For Zn-1.5 wt.% Al- 1.5 wt.% Mg coatings immersed in 0.1 mol.dm^{-3} acetic acid (HAc) a linear trend was observed between thickness and time before exposure of the underlying iron substrate.

- An inverse linear relationship was found to exist between Zn-1.5 wt.% Al- 1.5 wt.% Mg coating thickness and FFC propagation rate.

- These findings are consistent with the hypothesis that filiform advancement occurs via a penetrative through coating mechanism in which anodic dissolution of the Mg rich phases (primarily $MgZn_2$) allows O_2 percolation to Fe substrate, which acts as the FFC cathode. The exposed iron is then able to galvanically couple to the ZAM coating, increasing the driving force for filament advance. In the case of thicker coatings, the increased charge required for dissolution will result in reduced rates of propagation.

- For all ZAM coating compositions (1-6 wt. % Al, 1-3 wt. % Mg) EDS derived normalised coating Mg wt. % fell during immersion in 0.1 $mol.dm^{-3}$ HAc. As initial coating Al wt. % was increased, the decrease in Mg wt. %, and increase in substrate iron exposure (indicated by Fe wt. %) occurred less rapidly.

- The decreased rate of FFC observed in the case of coatings with higher Al content is consistent with the hypothesis that FFC propagates via coating dissolution mechanism. It is believed that the presence of increased Al (which does not dissolve in HAc) creates a more torturous route to the iron substrate following dissolution of the Mg rich phases.

- Although HAc, known to initiate FFC, is ubiquitous within indoor environments, HAc induced FFC is yet to be observed on ZAM in service. It seems plausible that the exact composition of ZAM may be modified in such a way as to decrease the rate of FFC propagation in the case that it should occur.

5. Acknowledgments

The authors would like to thank Tata Steel for providing samples and EPSRC for the funding for the Engineering Doctorate studentship via the Collaborate Training Account (GR/T11333/01).

The raw/processed data required to reproduce these findings cannot be shared at this time as the data also forms part of an ongoing study.

6. References

1. D. Thierry, D. Persson, G. Luckeneder, K. H. Stellnberger, Atmospheric corrosion of ZnAlMg coated steel during long term atmospheric weathering at different worldwide exposure sites, Corrosion Science. 148 (2019) 338-354. https://doi.org/10.1016/j.corsci.2018.12.033.

2. G.Williams, H. N.McMurray, Underfilm/coating corrosion, in: B. R. A. Cottis,M. Graham, R. Lindsay, S. Lyon, T. J. A. Richardson, D. J. D. Scantlebury, H. Stott, (Eds.), Shreir's Corrosion, Elsevier Science, 2009, pp. .988-2004.

3. A. Leng, H. Streckel, M. Stratmann, The delamination of polymeric coatings from steel. Part 1: Calibration of the Kelvinprobe and basic delamination mechanism, Corrosion Science. 41 (1999) 547-578. https://doi.org/10.1016/S0010-938X(98)00166-8.

4. A. Leng, H. Streckel, and M. Stratmann, The delamination of polymeric coatings from steel. Part 2: First stage of delamination, effect of type and concentration of cations on delamination, chemical analysis of the interface, Corrosion Science. 41 (1999) 579-597. https://doi.org/10.1016/S0010-938X(98)00167-X.

5. G. Williams, H.N. McMurray, Chromate Inhibition of Corrosion-Driven Organic Coating Delamination Studied Using a Scanning Kelvin Probe Technique, Journal of the Electrochemical Society. 148 (2001) B377-B385. https://doi.org/ doi:10.1149/1.1396336.

6. W. Furbeth, M. Stratmann, Investigation of the delamination of polymer films from galvanized steel with the Scanning Kelvinprobe, Fresenius' Journal of Analytical Chemistry. 353, 337 (1995) 337-341. https://doi.org/10.1007/BF00322064.

7. W. Furbeth, M. Stratmann, The delamination of polymeric coatings from electrogalvanised steel – a mechanistic approach.: Part 1: delamination from a defect with intact zinc layer, Corrosion Science. 43 (2001) 207-227. https://doi.org/10.1016/S0010-938X(00)00047-0.

8. W. Furbeth, M. Stratmann, The delamination of polymeric coatings from electrogalvanized steel – a mechanistic approach.: Part 2: delamination from a defect down to steel, Corrosion Science. 43 (2001) 229-241. https://doi.org/10.1016/S0010-938X(00)00048-2.

9. W. Furbeth, M. Stratmann, The delamination of polymeric coatings from electrogalvanized steel – a mechanistic approach.: Part 3: delamination kinetics and influence of CO2, Corrosion Science. 43 (2001) 243-254. https://doi.org/10.1016/S0010-938X(00)00049-4.

10. J. Sullivan, N. Cooze, C. Gallagher, T. Lewis, T. Prosek, D. Thierry, In situ monitoring of corrosion mechanisms and phosphate inhibitor surface deposition during corrosion of zinc–magnesium–aluminium (ZMA) alloys using novel time-lapse microscopy, Faraday Discussions. 180 (2015) 361-379. https://doi.org/ 10.1039/C4FD00251B.

11. J.H. Sullivan, S. Mehraban, J. Elvins, In situ monitoring of the microstructural corrosion mechanisms of zinc–magnesium–aluminium alloys using time lapse microscopy,Corrosion Science. 53 (2011) 2208-2215. https://doi.org/10.1016/j.corsci.2011.02.043.

12. M. Arndt, J. Duchoslav, H. Itani, G. Hesser, C.K. Riener, G. Angeli, K. Preis, D. Stifter, K. Hingerl, Nanoscale analysis of surface oxides on ZnMgAl hot-dip-coated steel sheets, Analytical and Bioanalytical Chemistry. 403 (2012) 651-661. https://doi.org/10.1007/s00216-011-5507-0.

13. C. Commenda, J. Pühringer, Microstructural characterization and quantification of Zn–Al–Mg surface coatings, Materials Characterization. 61 (2010) 943-951. https://doi.org/10.1016/j.matchar.2010.06.008.

14. R. Hausbrand, M. Stratmann, M. Rohwerder, Corrosion of zinc–magnesium coatings: Mechanism of paint delamination, Corrosion Science. 51 (2009) 2107-2114. https://doi.org/10.1016/j.corsci.2009.05.042.

15. R. Hausbrand, M. Stratmann, M. Rohwerder, The Physical Meaning of Electrode Potentials at Metal Surfaces and Polymer/Metal Interfaces: Consequences for Delamination Corrosion, Passivation, and Anodic Films, Journal of the Electrochemical Society. 155 (2008) C369-C379.https://doi.org/10.1149/1.2926589.17.

16. A. Vimalanandan, A. Bashir, M. Rohwerder, Zn-Mg and Zn-Mg-Al alloys for improved corrosion protection of steel: Some new aspects, Materials and Corrosion. 65 (2014) 392-400. https://doi.org/10.1002/maco.201307586.

17. R. Hausbrand, M. Stratmann, M. Rohwerder, Delamination Resistant Zinc Alloys: Simple Concept and Results on the System Zinc-Magnesium, Steel Res. Int. 74 (2003) 453-458. https://doi.org/10.1002/srin.200300212.

18. N. Wint, D. Eaves, E. Michailidou, A. Bennett, J.R. Searle, G. Williams, H.N. McMurray, The kinetics and mechanism of filiform corrosion occurring on zinc-aluminium-magnesium coated steel, Corrosion Science. 158 (2019) 108073. https://doi.org/10.1016/j.corsci.2019.06.028.

19. A. Bautista, Filiform corrosion in polymer-coated metals, Progress in Organic Coatings. 28 (1996) 49-58. https://doi.org/10.1016/0300-9440(95)00555-2.

20. R. T. Ruggeri and T. R. Beck, An Analysis of Mass Transfer in Filiform Corrosion, Corrosion-NACE. 39 (1983) 452-465. https://doi.org/10.5006/1.3581907.

21. G. Grundmeier, W. Schmidt, and M. Stratmann, Corrosion protection by organic coatings: electrochemical mechanism and novel methods of investigation,

Electrochimica Acta. 45 (2000) 2515-2533. https://doi.org/10.1016/S0013-4686(00)00348-0.

22. G. Williams, H.N. McMurray, The mechanism of group (I) chloride initiated filiform corrosion on iron, Electrochemistry Communications. 5 (2003) 871-877. https://doi.org/10.1016/j.elecom.2003.08.008.

23. T. M.Watson, A. J. Coleman, G.Williams, and H. N. McMurray, The effect of oxygen partial pressure on the filiform corrosion of organic coated iron, Corrosion Science. 89 (2014) 46-58. https://doi.org/10.1016/j.corsci.2014.08.004.

24. W.H. Slabaugh, M. Grotheer, Mechanism of Filiform Corrosion, Industrial & Engineering Chemistry. 46 (1954) 1014-1016. https://doi/pdf/10.1021/ie50533a053.

25. W. Schmidt and M. Stratmann, Scanning kelvinprobe investigations of filiform corrosion on aluminum alloy 2024-t3, Corrosion Science. 40 (1998) 1441-1443. https://doi.org/10.1016/S0010-938X(98)00044-4.

26. J. H. W. de Wit, New knowledge on localized corrosion obtained from local measuring techniques, Electrochimica Acta. 46 (2001) 3641-3650. https://doi.org/10.1016/S0013-4686(01)00642-9.

27. N. LeBozec, D. Persson, D. Thierry, S.B. Axelsen, Effect of Climatic Parameters on Filiform Corrosion of Coated Aluminum Alloys, CORROSION. 60 (2004) 584-593. https://doi.org/10.5006/1.3287763.

28. G. Williams, H.N. McMurray, The Kinetics of Chloride-Induced Filiform Corrosion on Aluminum Alloy AA2024-T3, Journal of The Electrochemical Society. 150 (2003) B380-B388. https://doi:10.1149/1.1589020.

29. H.N. McMurray, G. Williams, S. O'Driscoll, Chromate Inhibition of Filiform Corrosion on Organic Coated AA2024-T3 Studied Using the Scanning Kelvin Probe, Journal of the Electrochemical Society. 151 (2004) B406-B414. https://doi.org/10.1149/1.1757460.

30. H.N. McMurray, A. Holder, G. Williams, G.M. Scamans, A.J. Coleman, The kinetics and mechanisms of filiform corrosion on aluminium alloy AA6111, Electrochimica Acta. 55 (2010) 7843-7852. https://doi.org/10.1016/j.electacta.2010.04.035.

31. J.V. Kloet, W. Schmidt, A.W. Hassel, M. Stratmann, The role of chromate in filiform corrosion inhibition, Electrochimica Acta. 49 (2004) 1675-1685. https://doi.org/10.1016/S0013-4686(03)00256-1.

32. J.V. Kloet, W. Schmidt, A.W. Hassel, M. Stratmann, The role of chromate in filiform corrosion inhibition, Electrochimica Acta. 48 (2003) 1211-1222. https://doi.org/10.1016/S0013-4686(02)00829-0.

33. G. Williams, R. Grace, Chloride-induced filiform corrosion of organic-coated magnesium, Electrochimica Acta. 56 (2011) 1894-1903. https://doi.org/10.1016/j.electacta.2010.09.005.

34. C. Leygraf, J. Hedberg, P. Qiu, H. Gil, J. Henriquez, C.M. Johnson, W.R. Whitney Award Lecture: Molecular In Situ Studies of Atmospheric Corrosion, CORROSION. 63 (2007) 715-721. https://doi.org/10.5006/1.3278420.

35. C.M. Johnson, E. Tyrode, C. Leygraf, Atmospheric Corrosion of Zinc by Organic Constituents: I. The Role of the Zinc/Water and Water/Air Interfaces Studied by Infrared Reflection/Absorption Spectroscopy and Vibrational Sum Frequency Spectroscopy, Journal of The Electrochemical Society. 153 (2006) B113-B120. https://doi.org/10.1149/1.2164788.

36. C.M. Johnson, C. Leygraf, Atmospheric Corrosion of Zinc by Organic Constituents: II. Reaction Routes for Zinc-Acetate Formation, Journal of The Electrochemical Society. 153 (2006) B542-B546. https://doi.org/10.1149/1.2360740.

37. H. Gil, C. Leygraf, J. Tidblad, GILDES Model Simulations of the Atmospheric Corrosion of Zinc Induced by Low Concentrations of Carboxylic Acids, Journal of The Electrochemical Society. 159 (2012) C123-C128. https://doi.org/10.1149/2.072203jes.

38. P. Qiu, D. Persson, C. Leygraf, Initial Atmospheric Corrosion of Zinc Induced by Carboxylic Acids: A Quantitative In Situ Study, Journal of The Electrochemical Society. 156 (2009) C441-C447. https://doi.org/10.1149/1.3240878.

39. J. Hedberg, S. Baldelli, C. Leygraf, E. Tyrode, Molecular Structural Information of the Atmospheric Corrosion of Zinc Studied by Vibrational Spectroscopy Techniques: I. Experimental Approach, Journal of The Electrochemical Society. 157 (2010) C357-C362. https://doi.org/10.1149/1.3479207.

40. J. Hedberg, S. Baldelli, C. Leygraf, Molecular Structural Information of the Atmospheric Corrosion of Zinc Studied by Vibrational Spectroscopy Techniques: II. Two and Three-Dimensional Growth of Reaction Products Induced by Formic and Acetic Acid, Journal of The Electrochemical Society. 157 (2010) C363-C373. https://doi.org/10.1149/1.3479255.

41. D. Persson, C. Leygraf, Metal Carboxylate Formation during Indoor Atmospheric Corrosion of Cu, Zn, and Ni, Journal of The Electrochemical Society. 142 (1995) 1468-1477.https://doi.org/10.1149/1.2048598.

42. E. Johansson, C. Leygraf, B. Rendahl, Characterisation of corrosivity in indoor atmospheres with different metals and evaluation techniques, British Corrosion Journal. 33 (1998) 59-66. https://doi.org/10.1179/000705998798114769.

43. C. Vargel, Chapter F.6 - Carboxylic Acids and their Derivatives, in: C. Vargel (Ed), Corrosion of Aluminium, Elsevier, 2004, pp. 513-541.

44. A. Apelblat, E. Manzurola, Solubilities of magnesium, calcium, barium, cobalt, nickel, copper, and zinc acetates in water from T= (278.15 to 348.15) K, The Journal of Chemical Thermodynamics. 31(1999) 1347-1357.

45. H. M. Leung, S. D. Pike, A. J. Clancy, H. Chun Yau, W. Jun Lee, K. L. Orchard, M. S. P. Shaffer, C. K. Williams, Layered zinc hydroxide monolayers by hydrolysis of organozincs, Chemical Science. 9 (2018) 2135-2146. https://doi.org/10.1039/C7SC04256F.

46. J. Elvins, J.A Spittle, J.H. Sullivan, D.A. Worsley, The effect of magnesium additions on the microstructure and cut edge corrosion resistance of zinc aluminium alloy galvanised steel, Corrosion Science. 50 (2008) 1650-1658. https://doi.org/10.1016/j.corsci.2008.02.005.

47. R. Krieg, A. Vimalanandan, M. Rohwerder, Corrosion of Zinc and Zn-Mg Alloys with Varying Microstructures and Magnesium Contents. Journal of the Electrochemical. Society. **161** (2014) C156.

48. J. Elvins, J. A. Spittle, D. A. Worsley, Microstructural changes in zinc aluminium alloy galvanising as a function of processing parameters and their influence on corrosion, Corrosion Science. 47 (2005) 2740-2759. https://doi.org/10.1016/j.corsci.2004.11.011.

49. T. Prosek, J. Hagström, D. Persson, N. Fuertes, F. Lindberg, O. Chocholatý, C. Taxén, J. Šerák, D. Thierry, Effect of the microstructure of Zn-Al and Zn-Al-Mg model alloys on corrosion stability, Corrosion Science. 110 (2016) 71-81. https://doi.org/10.1016/j.corsci.2016.04.022.

50. P. Volovitch, T. N. Vu, C. Allely, A. A. Aal, K. Ogle, Understanding corrosion via corrosion product characterization: II. Role of alloying elements in improving the corrosion resistance of Zn–Al–Mg coatings on steel, Corrosion Science. 53 (2011) 2437-2445. https://doi.org/10.1016/j.corsci.2011.03.016.

51. X. Zhang, T. N. Vu, P. Volovitch, C. Leygraf, K. Ogle, I. Odnevall Wallinder, The initial release of zinc and aluminium from non-treated Galvalume and the formation of corrosion products in chloride containing media, Applied Surface Science. 258 (2012) 4351-4359. https://doi.org/10.1016/j.apsusc.2011.12.112.

52. J. Duchoslav, M. Arndt, R. Steinberger, T. Keppert, G. Luckeneder, K.H. Stellnberger, J. Hagler, C.K. Riener, G. Angeli, D. Stifter, Nanoscopic view on the initial stages of corrosion of hot dip galvanized Zn–Mg–Al coatings, Corrosion Science. 83 (2014) 327-334. https://doi.org/10.1016/j.corsci.2014.02.027.

53. T.N. Vu, P. Volovitch, K. Ogle, The effect of pH on the selective dissolution of Zn and Al from Zn–Al coatings on steel, Corrosion Science. 67 (2013) 42-29. https://doi.org/10.1016/j.corsci.2012.09.042.

54. M. Salgueiro Azevedo, C. Allely, K. Ogle, P. Volovitch, Corrosion mechanisms of Zn(Mg,Al) coated steel: 2. The effect of Mg and Al alloying on the formation and

properties of corrosion products in different electrolytes, Corrosion Science. 90, (2015) 482-490. https://doi.org/10.1016/j.corsci.2014.07.042.

55. T. Prosek, D. Persson, J. Stoulil, D. Thierry, Composition of corrosion products formed on Zn–Mg, Zn–Al and Zn–Al–Mg coatings in model atmospheric conditions, Corrosion Science. 86 (2014) 231-238. https://doi.org/10.1016/j.corsci.2014.05.016.

56. J.D. Yoo, P. Volovitch, A.A. Aal, C. Allely, K. Ogle, The effect of an artificially synthesized simonkolleite layer on the corrosion of electrogalvanized steel, Corrosion Science. 70 (2013) 1-10. https://doi.org/10.1016/j.corsci.2012.10.024.

57. P. Volovitch, M. Serdechnova, K. Ogle, Aqueous Corrosion of Mg-Al Binary Alloys: Roles of Al and Mg, Corrosion. 68 (2012) 557-570. https://doi.org/10.5006/i0010-9312-68-6-557.

58. T. Lostak, A. Maljusch, B. Klink, S. Krebs, M. Kimpel, J. Flock, S. Schulz, W. Schuhmann, Zr-based conversion layer on Zn-Al-Mg alloy coated steel sheets: insights into the formation mechanism, Electrochimica Acta. 137 (2014) 65-74. https://doi.org/10.1016/j.electacta.2014.05.163.

59. B. Schuhmacher, C. Schwerdt, U. Seyfert, O. Zimmer, Innovative steel strip coatings by means of PVD in a continuous pilot line: process technology and coating development, Surface and Coatings Technology. 163. (2003) 703-709. https://doi.org/10.1016/S0257-8972(02)00660-6,

60. J.L. Davies, C.F. Glover, J. Van de Langkruis, E. Zoestbergen, G. Williams, The effect of Mg concentration on the resistance of PVD Zn-Mg coatings to corrosion driven organic coating delamination, Corrosion Science. 100 (2015) 607-618. https://doi.org/10.1016/j.corsci.2015.08.03.

61. J. Duchoslav, M. Arndt, T. Keppert, G. Luckeneder, D. Stifter, XPS investigation on the surface chemistry of corrosion products on ZnMgAl-coated steel, Analytical and Bioanalytical Chemistry. 405 (2013) 7133-7144. https://doi.org/10.1007/s00216-013-7099-3).

62. S. Schuerz, M. Fleischanderl, G. H. Luckeneder, K. Preis, T. Haunschmied, G. Mori, A.C. Kneissl, Corrosion behaviour of Zn–Al–Mg coated steel sheet in sodium chloride-containing environment, Corrosion Science. 51 (2009) 2355-2363. https://doi.org/10.1016/j.corsci.2009.06.019.

63. T. Prosek, N. Larche, M. Vlot, F. Goodwin, D. Thierry, Corrosion performance of Zn–Al–Mg coatings in open and confined zones in conditions simulating automotive applications, Materials and Corrosion. 61 (2010) 412-420. https://doi.org/10.1002/maco.200905425.

64. L. Jiang, M. Wolpers, P. Volovitch, K. Ogle, Activation and inhibition of Zn–Al and Zn–Al–Mg coatings on steel by nitrate in phosphoric acid solution, Corrosion Science. 60 (2012) 256-264. https://doi.org/10.1016/j.corsci.2012.03.028.

65. T. Prosek, A. Nazarov, U. Bexell, D. Thierry, J. Serak, Corrosion mechanism of model zinc–magnesium alloys in atmospheric conditions, Corrosion Science. 50 (2008) 2216-2231. https://doi.org/10.1016/j.corsci.2008.06.008.

66. E. Diler, S. Rioual, B. Lescop,D. Thierry, B. Rouvellou,Chemistry of corrosion products of Zn and MgZn pure phases under atmospheric conditions, Corrosion Science. 65 (2012) 178-186. https://doi.org/10.1016/j.corsci.2012.08.014.

67. B. Li, A. Dong, G. Zhu, S. Chu, H. Qian, C. Hu, B. Sun, J. Wang, Investigation of the corrosion behaviors of continuously hot-dip galvanizing Zn-Mg coating, Surface and Coatings Technology. 206 (2012) 3989-3999. https://doi.org/10.1016/j.surfcoat.2012.03.079.

68. P. Volovitch, C. Allely, K. Ogle, Understanding corrosion via corrosion product characterization: I. Case study of the role of Mg alloying in Zn-Mg coating on steel, Corrosion Science. 51 (2009) 1251-1262. https://doi.org/10.1016/j.corsci.2009.03.005.

69. N. C. Hosking, M. A. Ström, P. H. Shipway, C. D. Rudd, Corrosion resistance of zinc-magnesium coated steel, Corrosion Science. 49 (2007) 3669-3695. https://doi.org/10.1016/j.corsci.2007.03.032.

70. P. Volovitch, T.N. Vu, C. Allély, A. Abdel Aal, K. Ogle, Understanding corrosion via corrosion product characterization: II. Role of alloying elements in improving the corrosion resistance of Zn–Al–Mg coatings on steel, Corrosion Science. 51 (2009) 2355-2363. https://doi.org/10.1016/j.corsci.2009.06.019.

71. N. LeBozec, D. Thierry, A. Peltola, L. Luxem, G. Luckeneder, G. Marchiaro, M. Rohwerder, Corrosion performance of Zn–Mg–Al coated steel in accelerated corrosion tests used in the automotive industry and field exposures, Materials and Corrosion. 64 (2013) 969-978. https://doi.org/10.1002/maco.201206959.

72. E. De Bruycker, Z. Zermout, B. C. De Cooman, Zn-Al-Mg Coatings: Thermodynamic Analysis and Microstructure Related Properties, Materials Science Forum. 539-543 (2007) 1276-1281. https://10.4028/www.scientific.net/MSF.

73. M. Vlot, M. Juijderwijk, M. Toose, L. Elliot, R. Bleeker, T. Maalman, Hot dip ZnAlMg coatings: Microstructure and forming properties, Galvatech 7th International Conference on Zinc and Zinc Alloy Coated Steel Sheet. (2007) 574-579.

74. C. F. Baes, R. E. Mesmer, The Hydrolysis of Cations, Wiley, New York (1976).

75. X. Zhang, C. Leygraf, I. O. Wallinder, Atmospheric corrosion of Galfan coatings on steel in chloride-rich environments, Corrosion Science. 73 (2013) 62-71.

76. R. Krieg, M. Rohwerder, S. Evers, B. Schuhmacher, J. Schauer-Pass, Cathodic self-healing at cut-edges: The effect of Zn2+ and Mg2+ ions, Corrosion Science. 65 (2012) 119-127. https://doi.org/10.1016/j.corsci.2012.08.008

7. Figure Legends

Figure 1. SEM backscatter images of the cross section of 1.5Al-1.5Mg coatings of various coating weights a.) 70 $g.m^{-2}$, b.) 100 $g.m^{-2}$, c.) 140 $g.m^{-2}$ d.) 200 $g.m^{-2}$, e.) 275 $g.m^{-2}$ and f.) 350 $g.m^{-2}$.

Figure 2. SEM backscatter images of the surface of a.) 1Al-1Mg , b.) 1.5Al-1.5Mg c.) 3Al-3Mg and d.) 6Al-3Mg coatings alongside corresponding EDS elemental (Fe) maps obtained after various times of immersion in 0.1 $mol.dm^{-3}$ HAc.

Figure 3. Normalised a.) Mg wt.%, b.) Al wt.% and c.) Fe wt.% obtained using EDS for ZAM coatings of various compositions after various times of immersion in 0.1 $mol.dm^{-3}$ HAc.

Figure 4. a.) Backscatter SEM images of both a 1Al-1Mg and 6Al-3Mg cross section obtained prior to and after 15 seconds immersed in 0.8 $mol.dm^{-3}$ HAc.

Figure 5. Time to iron substrate exposure when 1.5Al-1.5Mg coatings of varying thicknesses are immersed in 0.1$mol.dm^{-3}$ HAc at a temperature of 20°c

Figure 6. Optical images of FFC propagating on a.) 1Al-1Mg , b.) 1.5Al-1.5Mg c.) 3Al-3Mg and d.) 6Al-3Mg coated steel after 1 week, 4 weeks and 8 weeks after FFC has been initiated by injecting 2µL of 1.5 $mol.dm^{-3}$ HAc to a scribe defect.

Figure 7. The time dependent corroded area for the case that FFC is initiated on ZAM coatings of varying composition using 1.5 $mol.dm^{-3}$ HAc.

Figure 8. The time dependent corroded area for the case that FFC is initiated on 1.5Al-1.5Mg coatings of varying thickness using 1.5 $mol.dm^{-3}$ HAc.

Figure 9. FFC corroded area rate as a function of the reciprocal of 1.5Al-1.5Mg coating thickness.

8. Tables

Table 1. List of ZAM coatings used during systematic study of the effect of coating composition on susceptibility to FFC. Coating weight 140 $g.m^{-2}$, coating thickness ~ 10 µm.

Denomination	Zinc (wt. %)	Aluminium (wt. %)	Magnesium (wt. %)
Al1-Mg1	98	1	1
Al1.5-Mg1.5	97	1.5	1.5
Al3-Mg3	94	3	3
Al6-Mg3	91	6	3

Table 2. List of ZAM (1. 5Al-1.5Mg) coatings used during systematic study of the effect of coating weight (thickness) on susceptibility to FFC.

Coating weight (g.m^{-2})	Coating thickness (µm)
70	5
100	7
140	10
200	14
275	20
350	27

Table 3. SEM derived percentage of surface area covered by each phase present in each coating and EDS derived phase compositions.

Coating	Phase	Surface Area Percentage	Zn wt %	Al wt. %	Mg wt. %
1Al-1Mg	Primary Zinc	80	99.7	0.2	0.1
	Binary eutectic	10	95.9	0.5	3.6
	Ternary eutectic	10	91.9	4.0	4.1
	Zn-Al	0	/	/	/
1.5Al-1.5Mg	Primary Zinc	30	99.6	0.0	0.3
	Binary eutectic	30	95.1	0.7	4.2
	Ternary eutectic	40	90.6	4.0	4.4
	Zn-Al	0	/	/	/
3Al-3Mg	Primary Zinc	10	99.5	0.1	0.5
	Binary eutectic	30	94.8	0.5	4.7
	Ternary eutectic	50	89.8	7.4	3.8
	Zn-Al	10	80.6	19.3	0.1
6Al-3Mg	Primary Zinc	0	/	/	/
	Binary eutectic	10	95.4	0.5	4.1
	Ternary eutectic	70	89.7	3.9	6.4
	Zn-Al	20	79.2	21.7	0.0

Table 4. Average corroded area in the case that FFC is initiated using 1.5 mol.dm^{-3} HAc on varying compositions of ZAM coatings, along with corroded area rate.

Time (weeks)	Area (mm^2)			
	1Al-1Mg	**1.5Al-1.5Mg**	**3Al-3Mg**	**6Al-3Mg**
0	0	0	0	0
1	0.32±0.13	0.10±0.03	0.05+0.03	0.01±0.01
2	0.51±0.19	0.16±0.07	0.08±0.04	0.02±0.01
3	0.83±0.31	0.41±0.24	0.09±0.05	0.02±0.01
4	1.13±0.45	0.66±0.32	0.17±0.14	0.02±0.02
5	1.36±0.50	0.96±0.44	0.28±0.30	0.03±0.01
Area rate (mm^2.week^{-1})	0.28±0.01	0.27±0.01	0.10±0.01	0.05±0.01

Table 5. Average corroded area in the case that FFC is initiated using 1.5 mol.dm^{-3} HAc on 1.5Al-1.5Mg ZAM coatings of varying thickness, along with corroded area rate.

Time (weeks)	Area (mm^2)

	70 g.m^{-2}	**100 g.m^{-2}**	**140 g.m^{-2}**	**200 g.m^{-2}**	**275 g.m^{-2}**	**350 g.m^{-2}**
	5 µm	**7 µm**	**10 µm**	**14 µm**	**20 µm**	**27 µm**
0	0	0	0	0	0	0
1	0.20±0.08	0.15±0.08	0.10±0.03	0.03±0.02	0.03±0.01	0.02±0.01
2	0.56±0.25	0.38±0.09	0.16±0.07	0.07±0.05	0.08±0.03	0.03±0.02
3	0.82±0.27	0.62±0.15	0.41±0.24	0.21±0.18	0.16±0.09	0.04±0.02
4	1.20±0.43	0.93±0.23	0.66±0.32	0.43±0.30	0.33±0.14	0.12±0.10
5	1.54±0.54	1.19±0.34	0.96±0.44	0.76±0.47	0.48±0.23	0.25±0.12
Area rate (mm^2.week^{-1})	0.31±0.01	0.24±0.01	0.27±0.01	0.23±0.02	0.16±0.01	0.11±0.01

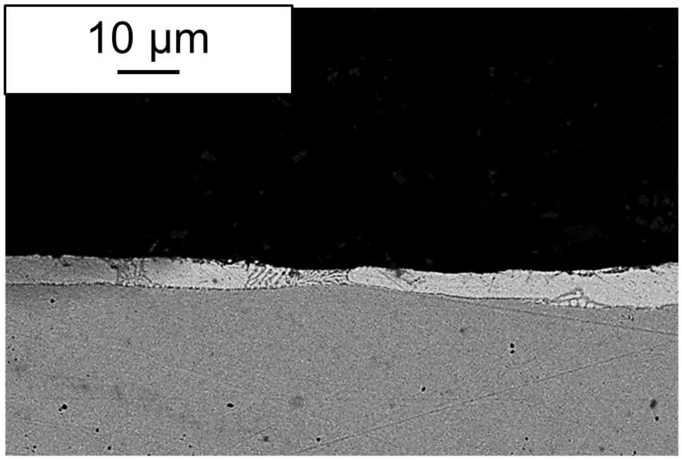

a.) 70 g.m^{-2}

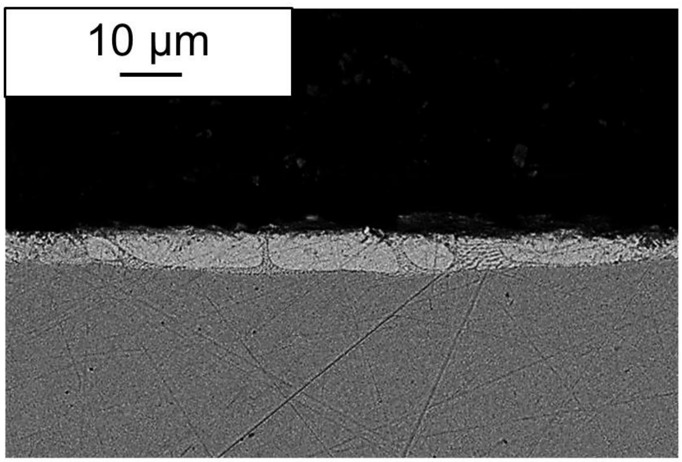

b.) 100 g.m^{-2}

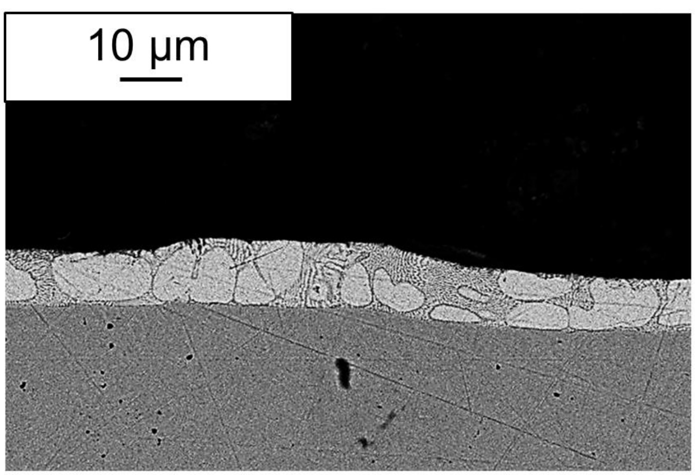

c.) 140 g.m^{-2}

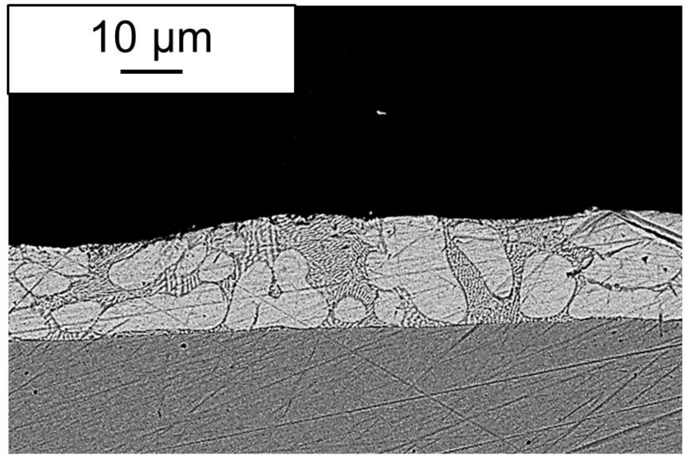

d.) 200 g.m^{-2}

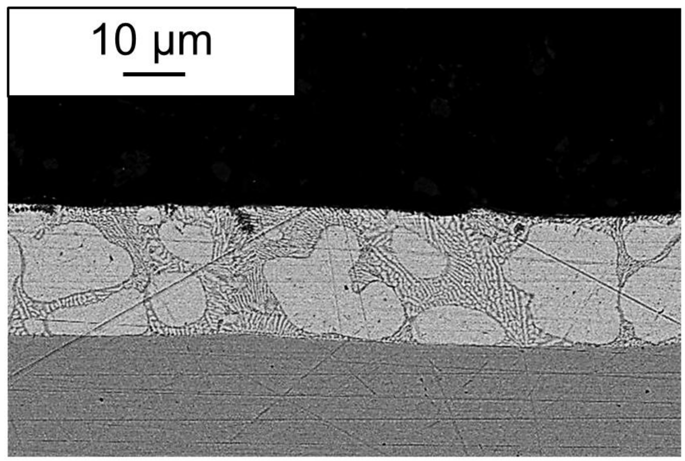

e.) 275 g.m^{-2}

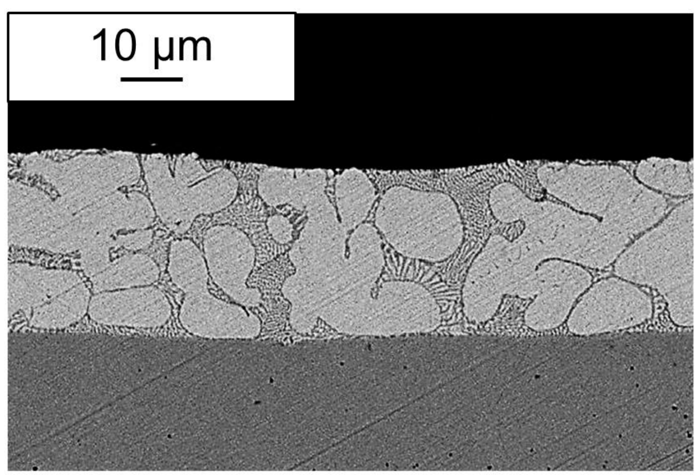

f.) 350 g.m^{-2}

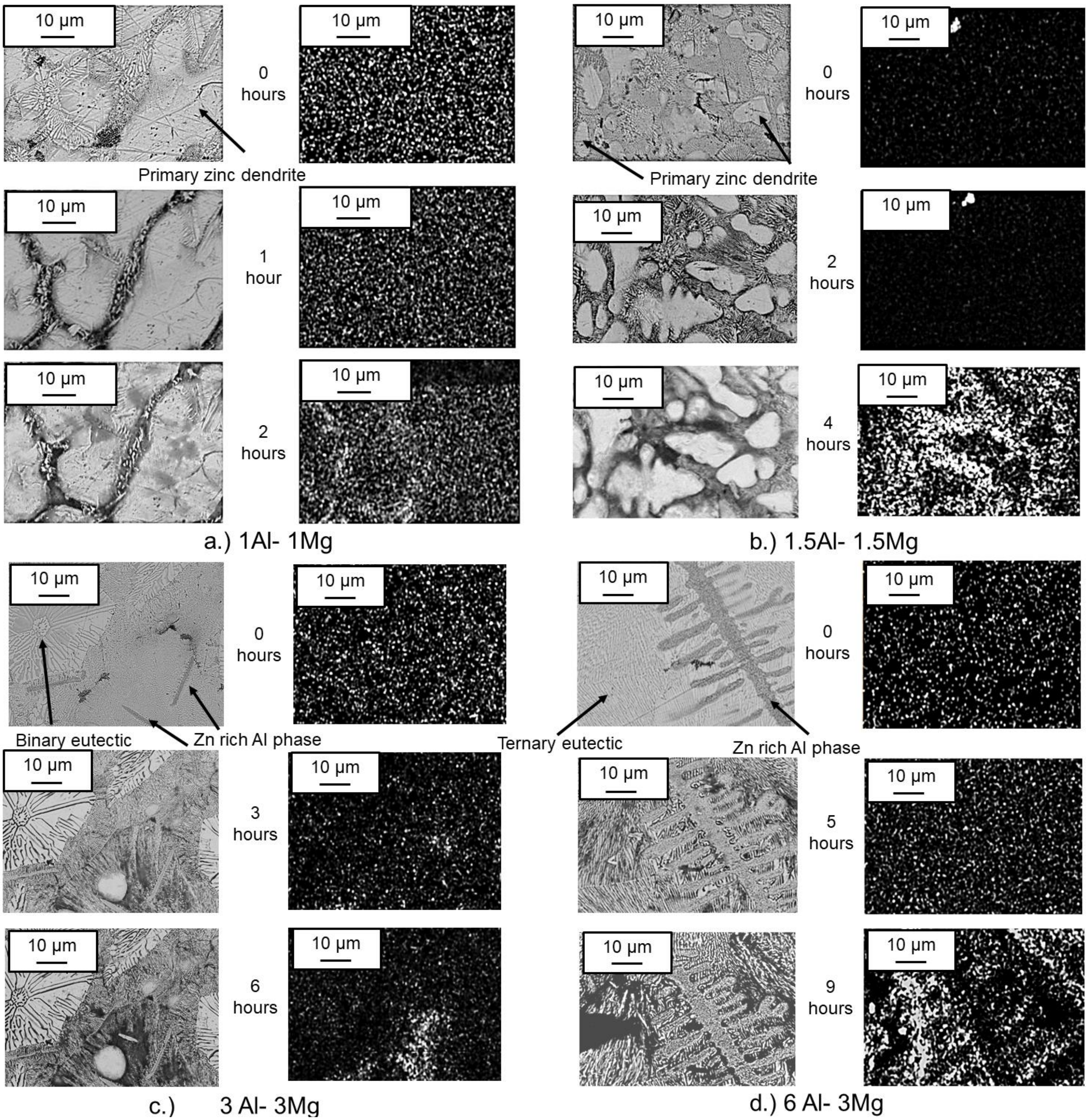
10 μm
0 hours
Primary zinc dendrite
1 hour
2 hours
a.) 1Al- 1Mg
4 hours
b.) 1.5Al- 1.5Mg
Binary eutectic
Zn rich Al phase
3 hours
6 hours
c.) 3 Al- 3Mg
Ternary eutectic
5 hours
9 hours
d.) 6 Al- 3Mg

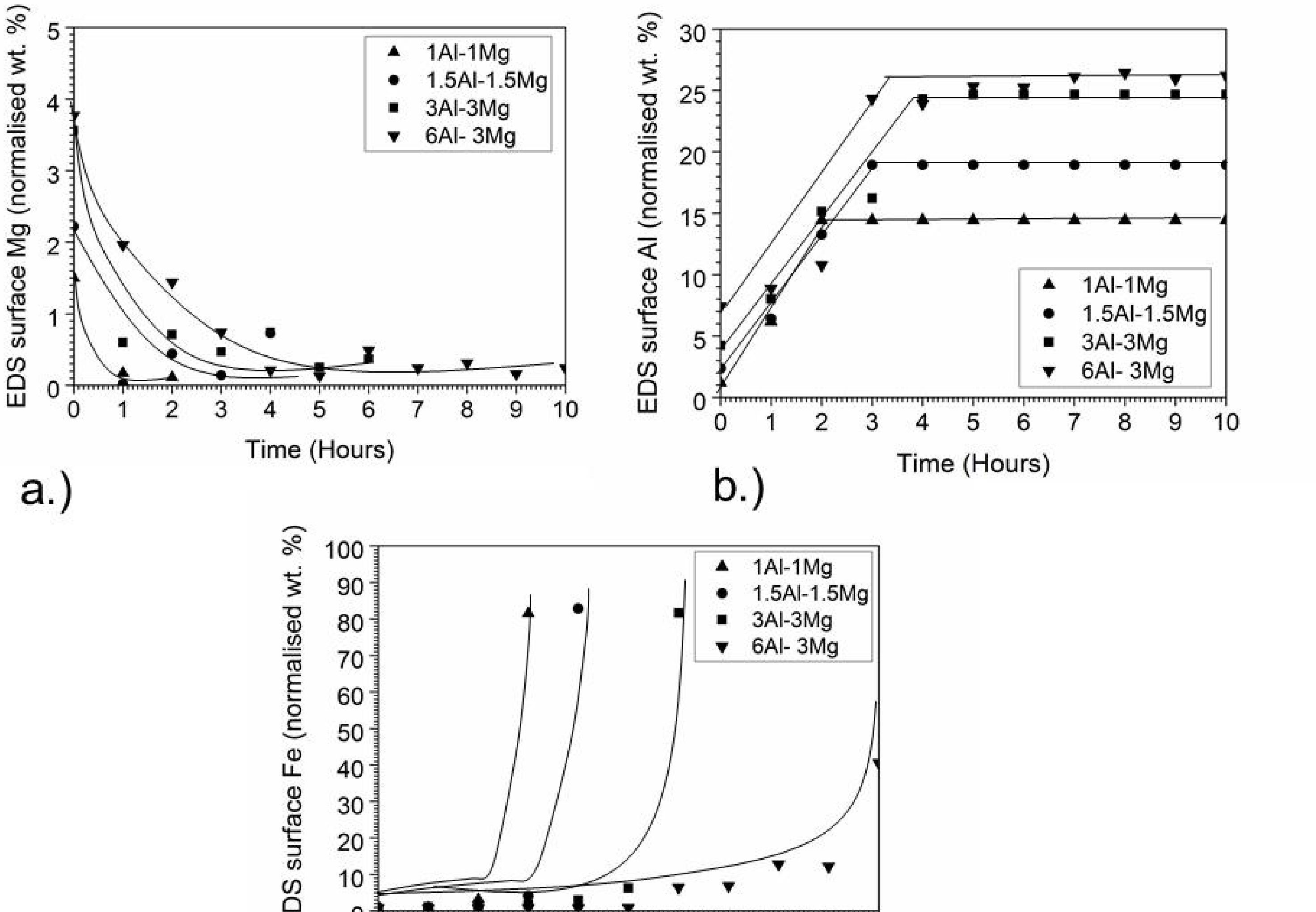

EDS surface Mg (normalised wt. %)
Time (Hours)
1Al-1Mg
1.5Al-1.5Mg
3Al-3Mg
6Al- 3Mg
a.)
EDS surface Al (normalised wt. %)
Time (Hours)
1Al-1Mg
1.5Al-1.5Mg
3Al-3Mg
6Al- 3Mg
b.)
EDS surface Fe (normalised wt. %)
Time (Hours)
1Al-1Mg
1.5Al-1.5Mg
3Al-3Mg
6Al- 3Mg
c.)

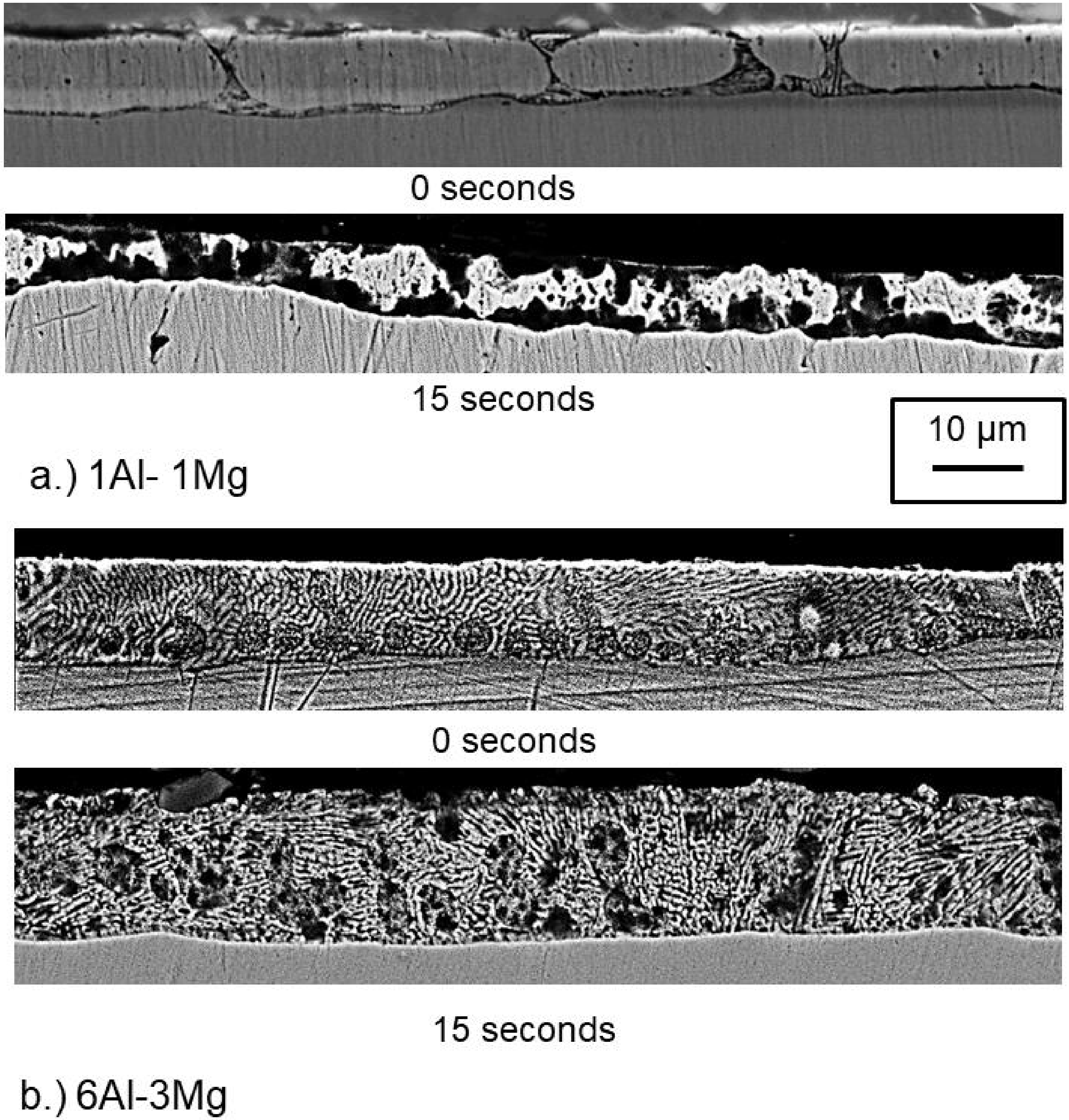
0 seconds
15 seconds
10 µm
a.) 1Al- 1Mg
0 seconds
15 seconds
b.) 6Al-3Mg

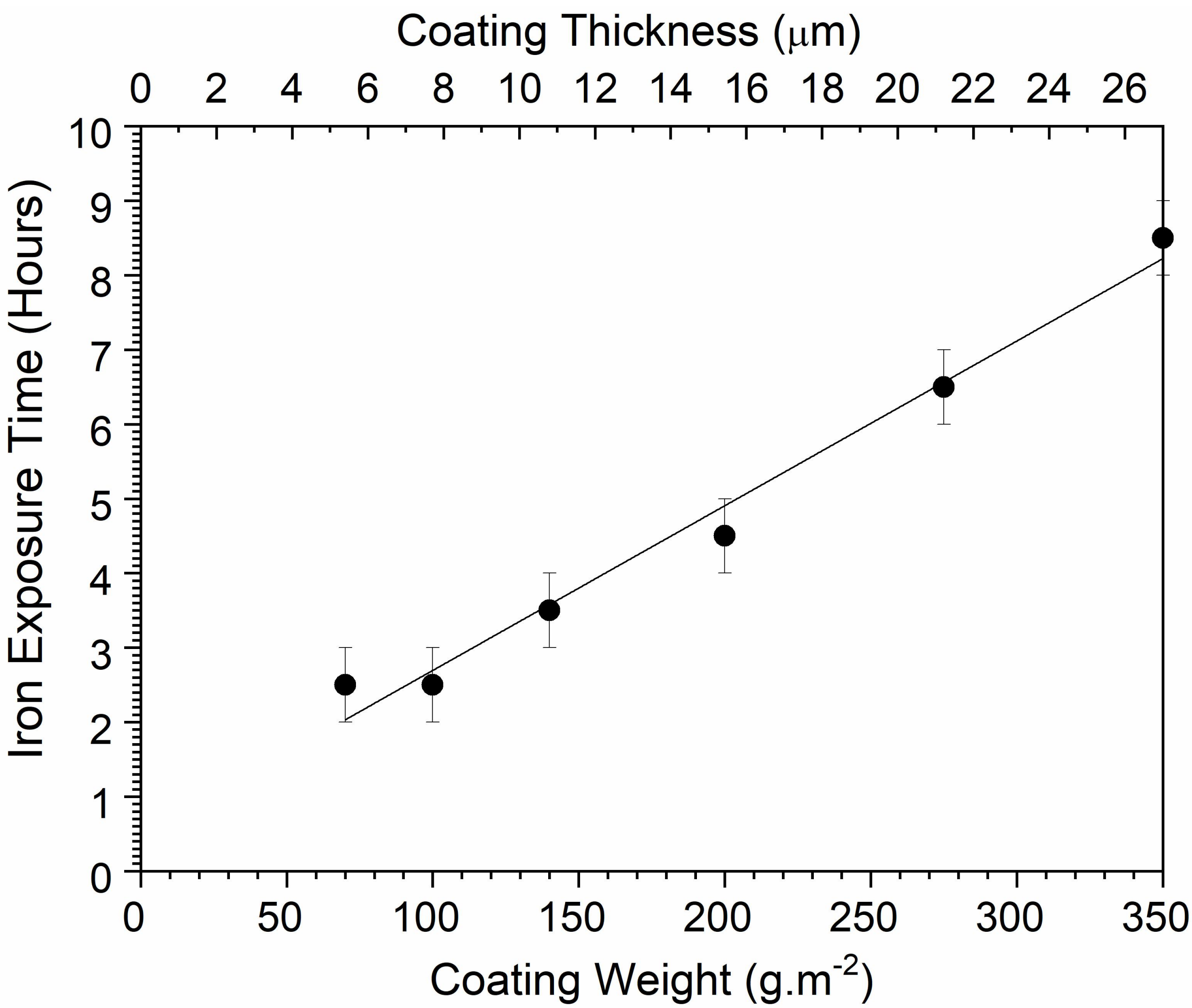
Coating Thickness (μm)
0 2 4 6 8 10 12 14 16 18 20 22 24 26
Iron Exposure Time (Hours)
0 1 2 3 4 5 6 7 8 9 10
0 50 100 150 200 250 300 350
Coating Weight (g.m-2)

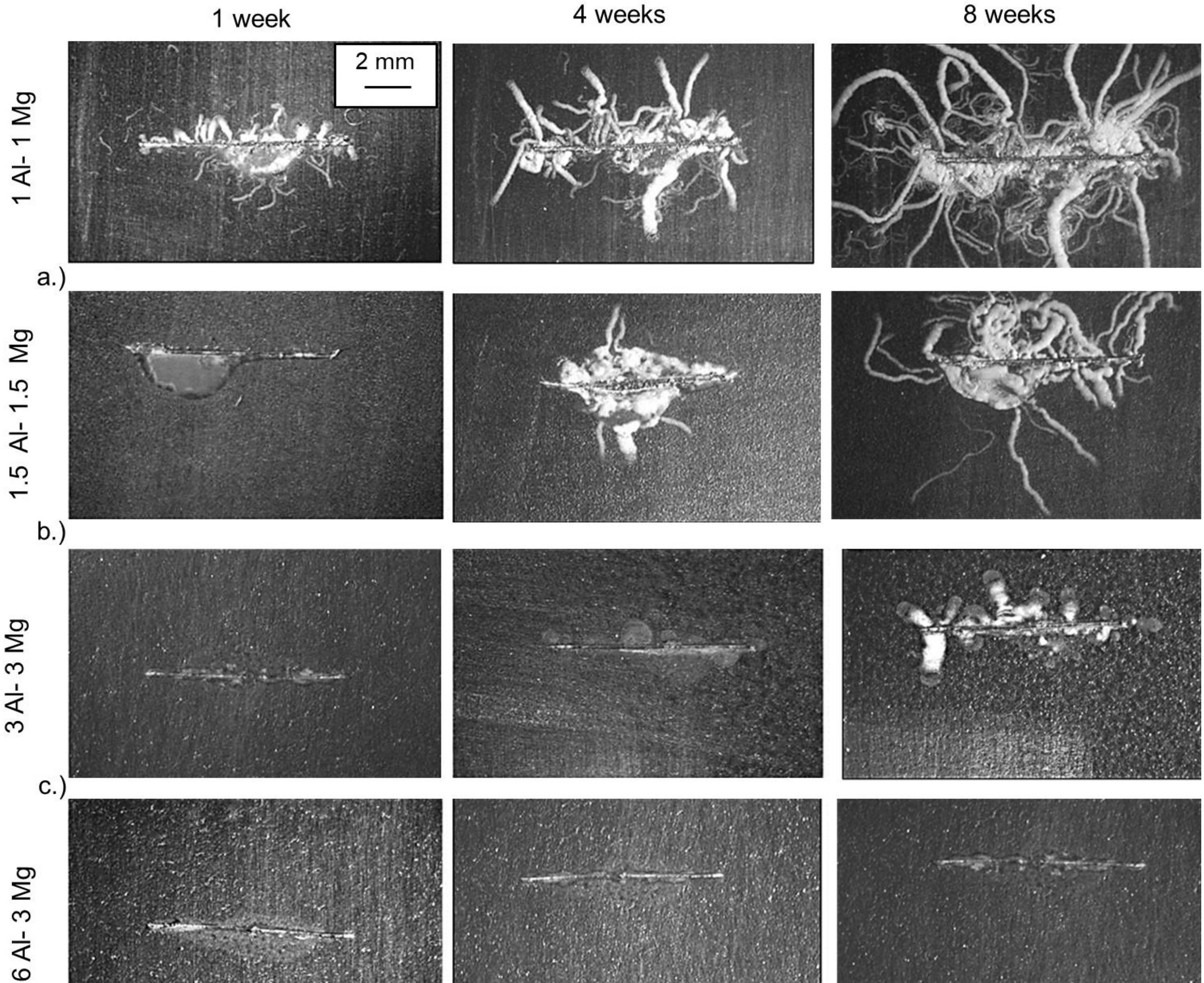
1 week
4 weeks
8 weeks
2 mm
1 Al- 1 Mg
a.)
1.5 Al- 1.5 Mg
b.)
3 Al- 3 Mg
c.)
6 Al- 3 Mg
d.)

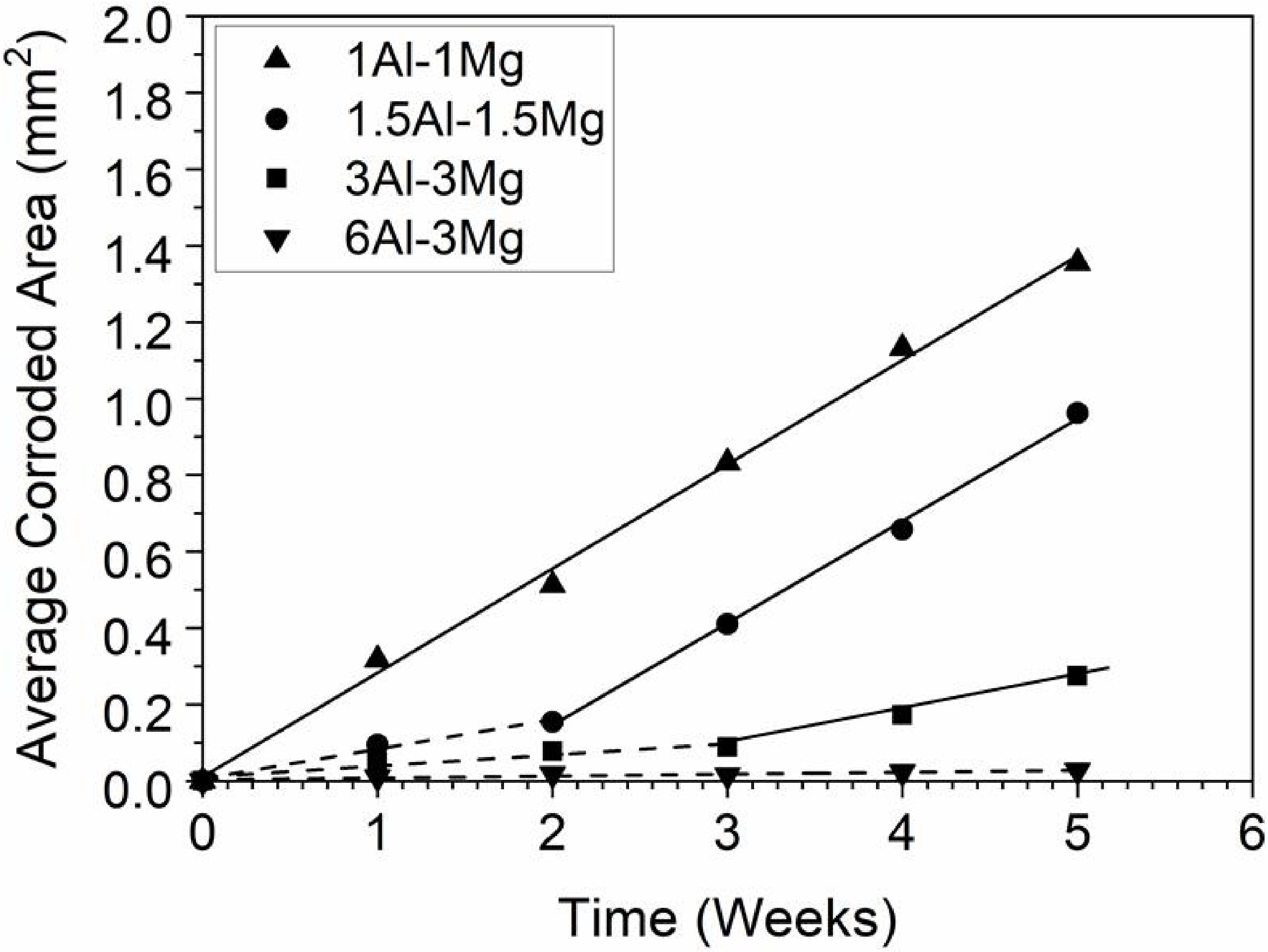

Average Corroded Area (mm2)
2.0
1.8
1.6
1.4
1.2
1.0
0.8
0.6
0.4
0.2
0.0
1Al-1Mg
1.5Al-1.5Mg
3Al-3Mg
6Al-3Mg
0
1
2
3
4
5
6
Time (Weeks)

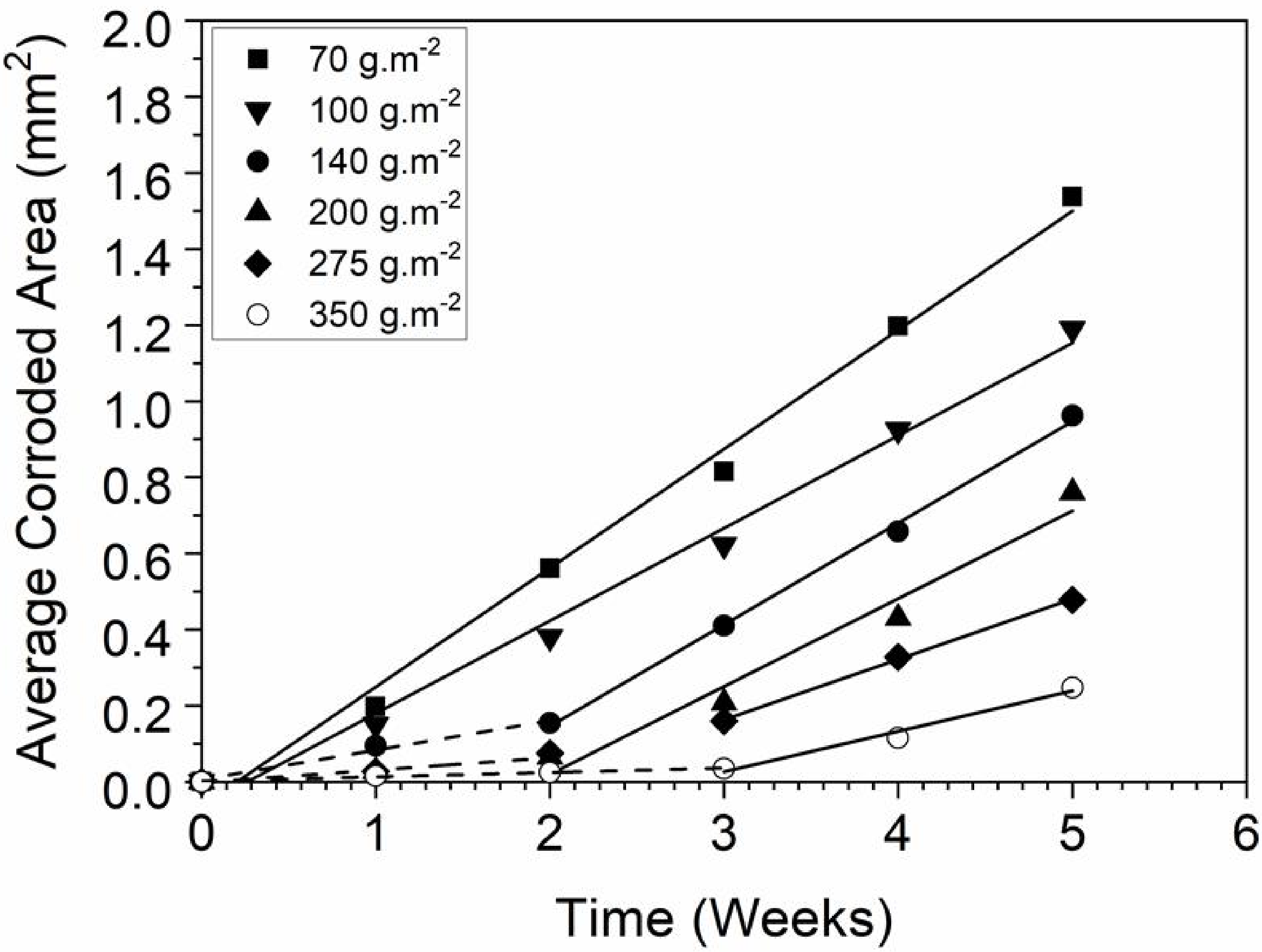

Average Corroded Area (mm2)
Time (Weeks)
70 g.m-2
100 g.m-2
140 g.m-2
200 g.m-2
275 g.m-2
350 g.m-2
0.0
0.2
0.4
0.6
0.8
1.0
1.2
1.4
1.6
1.8
2.0
0
1
2
3
4
5
6

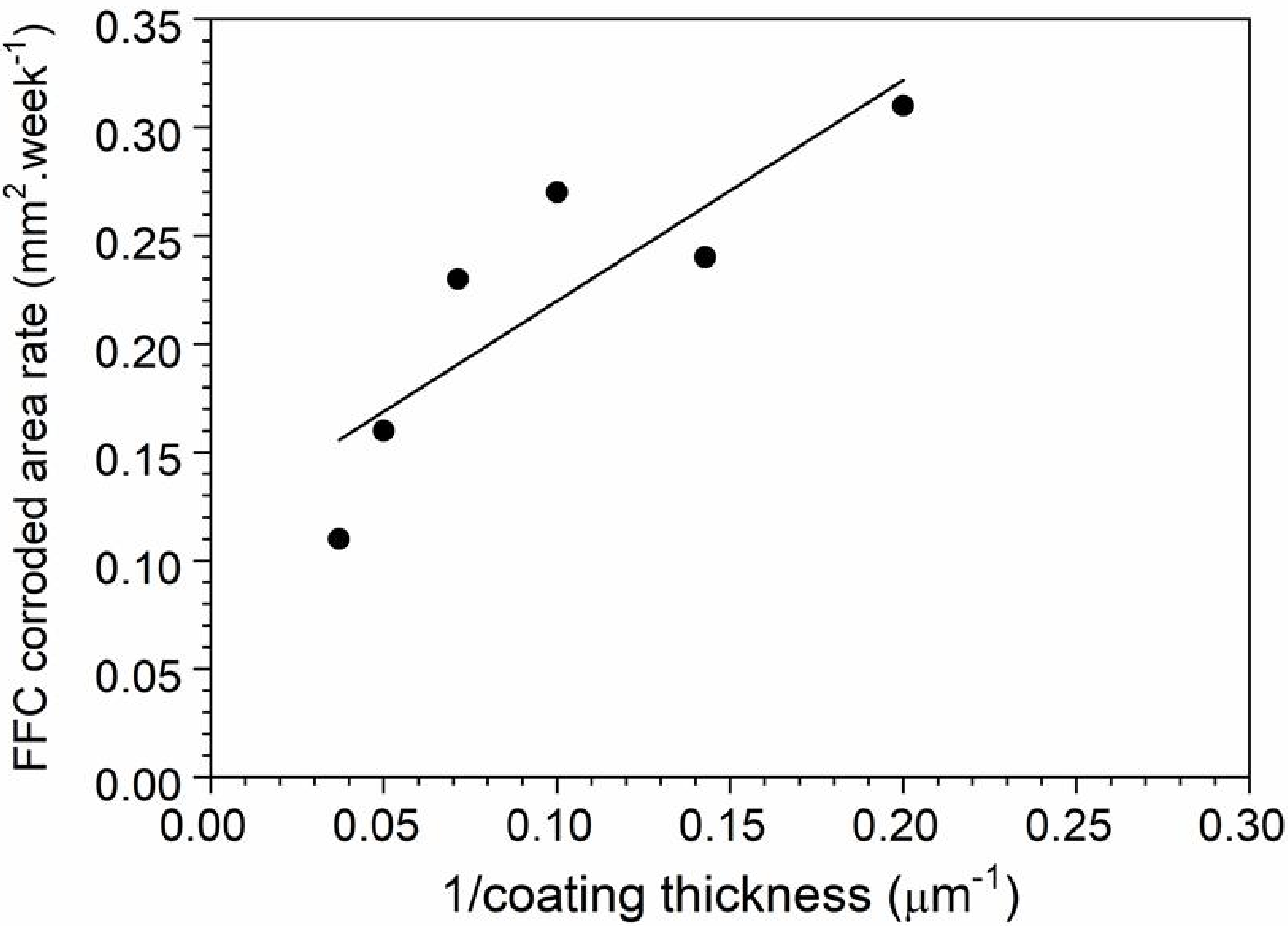
FFC corroded area rate (mm².week⁻¹)
0.35
0.30
0.25
0.20
0.15
0.10
0.05
0.00
0.00
0.05
0.10
0.15
0.20
0.25
0.30
1/coating thickness (μm⁻¹)